Uncertainty Considerations for the Comparison of Water Vapour Derived from Radiosondes and GNSS

Sz. Rózsa

Abstract

The integrated water vapour (IWV) can be estimated from the tropospheric delays of GNSS signals. These estimations are usually validated by radiosonde observations. However, very limited information is available on the precision of the IWV determined by radiosondes. In this paper the methodology of the computation of IWV retrieved from radiosonde data is revised using the atmospheric profiles of pressure, relative humidity and temperature. The formulae to calculate the uncertainty of the estimated values are derived, where the correlation of the neighbouring atmospheric layers is also taken into account. The results show that the mean uncertainty of the IWV from radiosonde observations reaches the level of ± 0.26 kg/m^2 in case of the Vaisala RS-92 radiosondes in Central and Eastern Europe. However, it increases to ± 0.7 to 0.8 kg/m^2 in summertime.Since the zenith hydrostatic delay (ZHD) must be modeled accurately to estimate the IWV from GNSS observations, the Saastamoinen, the Hopfield and the Black tropospheric delay models have been validated with ZHD values computed from radiosonde observations in Central Europe. Moreover some local models have also been derived in order to minimize the bias in IWV caused by the existing tropospheric models. In order to take the effect of the masses above the topmost level of the radiosonde profile in consideration, the International Standard Atmosphere has been used. Since the radiosonde observations terminate at different altitudes and pressure levels, which certainly affect the accuracy of the computed ZHD values, the omission error has been modeled with a simple exponential function. The results showed that the best ZHD model fitted to the radiosonde observations with the bias and standard deviation of $+0.8$ and ± 1.2 mm, respectively. This means that the GNSS derived IWV is biased by -0.1 kg/m^2. This value is approximately 50 % lower than the bias caused by the Saastamoinen model.Finally, the calculation of the scale factor between the zenith wet delay (ZWD) and the IWV is studied. Various models exist to determine this scale factor. There are models that derive the scale factor as a direct function of the surface temperature, while other models use a linear regression model of the surface temperature to compute the mean temperature of water vapour in the troposphere and derive the scale parameter from physical equations. Radiosonde profiles were used to test the two approached in Central and Eastern Europe. The results showed that the prior model showed no bias, while the latter one showed a relative bias of approximately 0.3 %.

Sz. Rózsa (✉)
Department of Geodesy and Surveying, Budapest University of Technology and Economics, Muegyetem rkp. 3, 1111 Budapest, Hungary
e-mail: szrozsa@agt.bme.hu

C. Rizos and P. Willis (eds.), *Earth on the Edge: Science for a Sustainable Planet*, International Association of Geodesy Symposia 139, DOI 10.1007/978-3-642-37222-3_9,

Keywords
GNSS meteorology • Integrated water vapour • Radiosonde observations

1 Introduction

GNSS pseudorange and phase range observations are affected by the atmospheric masses of the troposphere. GNSS Meteorology studies this tropospheric effect to derive meteorological parameters, like the integrated water vapour content of the atmosphere or the spatial distribution of the water vapour density in the troposphere. In order to quantify the tropospheric delays affecting the ranging observations, other systematic error sources like orbit and clock error of the satellites, ionospheric effects, receiver clock error and the antenna phase center offset and variations must be considered in data processing. The ionospheric effect and the satellite and receiver clock errors are removed considering as observable the double difference ionospherefree linear combination of the phase ranges. Ultra-Rapid satellite orbit products of the International GNSS Service (Dow et al. 2009) provide accurate satellite positions for the near-real time applications, while ground-based GNSS observations are provided by continuously operating GNSS stations. In Pacione and Vespe (2008) intercomparisons between results from different GPS processing schemes show a mean ZTD station bias at the level of ±6 mm with a related standard deviation of about 7–8 mm.

The zenith wet delay can be calculated from the ZTD by modeling the hydrostatic part of the delay as a function of the observed surface pressure. Afterwards the ZWD is usually converted to IWV with a scale factor (Bevis et al. 1992).

With the emerging dense continuously operating GNSS networks, it became feasible to monitor the atmospheric water vapour with unprecedented spatial and temporal resolution. The estimated IWV values are usually validated by radiosonde observations, since they provide "in situ" observations of the humidity, temperature and pressure along a vertical profile. Since the IWV is a linear function of the zenith wet delay and the GNSS based estimations are carried out using the zenith total delay of the satellite signals, the zenith hydrostatic delay must be calculated using surface meteorological observations. This paper focuses on three topics of the application of radiosonde observations in the GNSS based estimation of the IWV.

Firstly, the uncertainty of the IWV values computed from the radiosonde profiles is discussed. The knowledge of this uncertainty is necessary for the correct validation of the GNSS based IWV estimations using the radiosonde observations. The World Meteorological Organization launches radiosonde intercomparison campaigns, where the sondes of the various manufacturers are compared. Nash et al. (2011) showed that the observed mean error of the IWV derived by the studied radiosondes is between ±0.65 and ±1 kg/m^2 depending on the manufacturer. Liu et al. (2000) derived analytical formulae to estimate the mean error of the IWV, but in that study the correlation between the IWV of the neighboring atmospheric layers are neglected. In this paper a rigorous approach is introduced, which takes this correlation into account.

Secondly, radiosonde profiles can be applied to assess the accuracy of the various models used for the quantification of hydrostatic delays. Two local models are also introduced for the modeling of the hydrostatic delays, in order to achieve more accurate ZWD estimations.

Thirdly, radiosonde profiles are applied to assess the accuracy of the models used for the calculation of the scale parameter between the ZWD and IWV.

The first part of the paper introduces the methodology of the calculation of IWV using ZTD estimates obtained from GNSS observations. Afterwards the radiosonde observations used in this study are presented in Sect. 3. Section 4 introduces the calculation of ZHD, ZWD, IWV and the scale factor between the IWV and the ZWD using radiosonde observations. Uncertainty measures of these quantities are also given in this part of the paper.

The evaluation of the mathematical models used for the calculation of IWV based on the estimated ZTD is discussed in Sect. 5. Local models of the ZHD and the scale factor calculations are also introduced here.

These investigations are based on radiosonde observations of more than 17 years from Central and Eastern Europe. In total more than 276,000 radiosonde profiles are used in this study.

All these investigations contribute to the development of an optimal processing strategy applied in the estimation of the IWV in Hungary using GNSS observations Rózsa (2011).

2 The Estimation of Integrated Water Vapour from GNSS Observations

GNSS positioning is realized with the measurement of the travel time of the microwave signals between the satellite and the receiver. The satellite–receiver distance is computed as a product of the travel time and the speed of light, thus, the positioning is carried out using the trilateration technique.

However the propagation of GNSS signals is affected by both the ionosphere and the neutral atmosphere. The effect of the ionosphere can be eliminated using the ionosphere-free linear combination of the phase ranges on two different observation frequencies. The neutral atmosphere decreases the speed of the broadcasted signal due to the fact, that the refractive index is larger than one. The refractivity can be split into the dry and the wet refractivities up to the frequency of 30 GHz (Smith and Weintraub 1953):

$$N = k_1 \frac{p_d}{T} + k_2 \frac{e_v}{T} + k_3 \frac{e_v}{T^2} = N_d + N_w, \tag{1}$$

where T is the ambient temperature of air, p_d is the partial pressure of the dry air, e_v is the partial pressure of water vapour, N_d and N_w are the dry and the wet refractivities respectively, k_1, k_2 and k_3 are empirical constants with the values of $k_1 = 0.7760$ K/Pa, $k_2 = 0.704$ K/Pa and $k_3 = 0.03739 \times 10^5$ K^2/Pa respectively (Bevis et al. 1992).

Since the refractivity is larger than one, a delay is observed in the signal propagation (Hofmann-Wellenhof et al. 2008). This time delay is usually converted to an excess range, which is called the total tropospheric delay. Its value can be computed with the line integral of the refractivity along the path of the satellite signal (Thayer 1974):

$$TD = 10^{-6} \int_s N \, ds, \tag{2}$$

where TD is the tropospheric delay in metres.

In positioning solutions, the hydrostatic delay is computed in the zenith direction based on surface meteorological parameters either observed or computed from standard atmosphere models, while the wet delay is a parameter to solve for. These zenith delays are mapped to the satellite direction with the help of the mapping functions (Niell 1996; Boehm et al. 2006).

When a network of continuously operating reference stations (CORS) is available, and the positions of these stations are known, the zenith total delay (ZTD) can be estimated by processing the ionosphere-free linear combination of phase ranges with optimal accuracy (Dach et al. 2007). Pacione and Vespe (2008) showed that the ZTD can be estimated with the accuracy of ±7 mm using GNSS observations.

Since the IWV is highly correlated with the ZWD, the ZHD must be modeled (e.g., Saastamoinen 1972, 1973; Hopfield 1969; Black 1978). Thus, the wet delays can be computed by:

$$ZWD = ZTD - ZHD. \tag{3}$$

The ZWD can be expressed as a function of water vapour density (Rózsa et al. 2012):

$$ZWD = 10^{-6} R_v \left(k_2 - \frac{R_d}{R_v} k_1 \right) \int_{h_0}^{h_{tp}} \rho_v \, dz + 10^{-6} k_3 R_v \int_{h_0}^{h_{tp}} \frac{\rho_v}{T} \, dz, \tag{4}$$

where R_d and R_v are the specific gas constants of the water vapour and the dry air respectively, T is the ambient temperature, h_0 and h_{tp} are the altitudes of the GNSS antenna and the tropopause, respectively.

The integrated water vapour above the GNSS antenna is defined as the vertical integral of the water vapour density:

$$IWV = \int_{h_0}^{h_{tp}} \rho_v \, dz. \tag{5}$$

By introducing Eqs. (5) to (4), the relationship between the ZWD and the IWV can be expressed:

$$ZWD = 10^{-6} R_v \left(k_2 - \frac{R_d}{R_v} k_1 \right) IWV + 10^{-6} k_3 R_v \frac{IWV}{T_m}, \tag{6}$$

where T_m is the mean temperature of water vapour:

$$T_m = \frac{\int_{h_0}^{h_{tp}} \rho_v \, dz}{\int_{h_0}^{h_{tp}} \frac{\rho_v}{T} \, dz}. \tag{7}$$

It can be clearly seen in Eq. (6), that the ZWD can be converted to IWV using a simple scale factor:

$$Q = \frac{IWV}{ZWD} = \frac{10^6}{R_v \left(-\frac{R_d}{R_v} k_1 + k_2 + \frac{k_3}{T_m} \right)}. \tag{8}$$

Bevis et al. (1992) derived a linear function of the observed surface temperature to compute the value of T_m from approximately 9,000 North American radiosonde observations:

$$T_m = 72 + 0.72 T_s, \tag{9}$$

where both of the temperature values are expressed in Kelvin. In this model the scale factor (Q) is computed using Eq. (8). This approach is widely used in the practice of IWV estimation using GNSS observations.

However, Emardson and Derks (2000) proposed a polynomial model of the surface temperature to compute the value of the scale factor Q directly:

$$Q = \frac{1}{a_0 + a_1 \left(T_s - \overline{T} \right) + a_2 \left(T_s - \overline{T} \right)^2}, \tag{10}$$

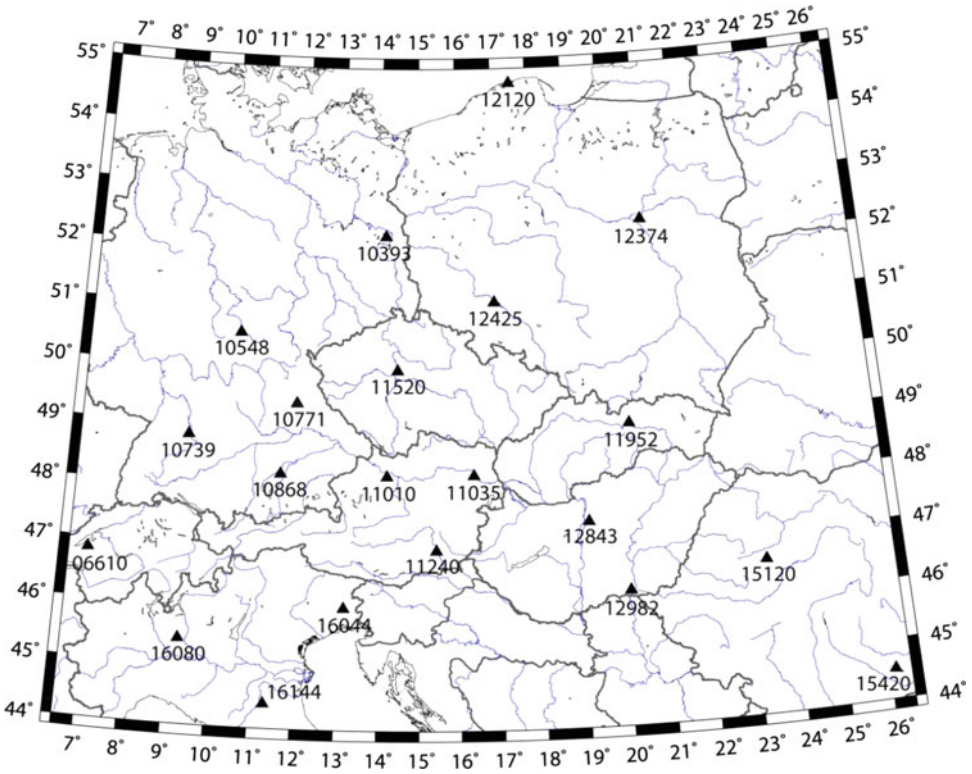

Fig. 1 The location of the radiosonde launch sites in Central and Eastern Europe used for this work

where the parameters a_0, a_1, a_2 and $\overline{T}$ are empirical constants derived from more than 100,000 radiosonde observations in Europe.

In this paper radiosonde observations are used to validate the functional models applied for the estimation of the IWV. The accuracy of the ZHD models and the determination of the scale factors are also studied. Based on local and regional radiosonde observations in Hungary and in Central Europe several models are derived and tested.

3 Radiosonde Data Used for This Study

Altogether more than 276,000 radiosonde observations profiles have been collected from 22 launching sites in Central and Eastern Europe from 01/01/1994 to 17/06/2011. Thus, more than 17 years of radiosonde observations have been analyzed in the study area (Fig. 1).

These data sets have been processed and various quantities have been computed, like the surface meteorological parameters, the burst altitude of the balloon, the topmost pressure level, the integrated water vapour, the tropospheric zenith delays (including hydrostatic and wet delays), the scale factor between the IWV and the ZWD values and the mean temperature of water vapour in the area.

4 The Computation of IWV and the Tropospheric Delays from Radiosonde Observations

This section discusses the IWV and the tropospheric delay computation from the temperature, air pressure and humidity profiles stemming from the radiosonde observations. In order to be able to assess the validation results correctly, the uncertainty of the IWV values must be considered. Thus, the methodology of the determination of these uncertainty values is also given.

4.1 The Computation of the IWV from Radiosonde Observations

The IWV can be computed from the observations of the temperature, air pressure and the humidity sensor of the sonde. The saturated water vapour pressure is calculated with the following equation (WMO 2008):

$$e_w = 6.112 \cdot e^{\frac{17.62T}{243.12+T}}, \tag{11}$$

where T is the ambient temperature in °C and e_w is the saturated water vapour pressure in hPa. Using the relative

humidity observation (RH) the partial pressure of water vapour (e_v) can be computed in hPa:

$$e_v = e_w \cdot RH. \tag{12}$$

Using the partial water vapour pressure and the total pressure (p), the mixing ratio (MR), which expresses the ratio between the mass of water vapour and the mass of the dry air (WMO 2008), is calculated:

$$MR = 621.98 \frac{e_v}{p - e_v}, \tag{13}$$

where e_v and p are expressed in hPa. The IWV in the atmospheric layers can be computed by integrating the mixing ratio with respect to the total air pressure:

$$IWV_i = \frac{1}{g}(p_{i-1} - p_i)\frac{MR_{i-1} + MR_i}{20}, \tag{14}$$

where IWV_i is the integrated water vapour in kg/m^2 in a layer bounded by the p_{i-1} and p_i pressure levels expressed in hPa, MR_{i-1} and MR_i are the mixing ratios at the lower and upper boundary of the layer respectively, while g is the gravity acceleration expressed in m/s^2.

The total IWV can be computed as the sum of the IWV in the various atmospheric layers in the troposphere.

Since the ambient temperature (T), the air pressure (p) and the dewpoint (T_d) are the observations, which are provided by the National Oceanic and Atmospheric Administration (NOAA) Global Radiosonde Database, the computation of the integrated water vapour must be slightly modified. The partial water vapour pressure can be computed directly from the dewpoint using the following equation:

$$e_v = 6.112 \cdot e^{\frac{17.62 T_d}{243.12 + T_d}}, \tag{15}$$

where e_v is the partial water vapour pressure in hPa and T_d is the dewpoint in °C. Afterwards Eqs. (13 and 14) must be used for the further computations.

4.2 The Uncertainty of the Computed IWV Values

GNSS-derived IWV estimates are usually compared to reference values retrieved from radiosonde observations. Recent studies show that the IWV estimates from GNSS observations agree with their radiosonde counterparts with a standard deviation of approximately (± 1.3 to 1.5) kg/m^2 (Bosy et al. 2010; Igondova and Cibulka 2010; Karabatic et al. 2011; Rózsa et al. 2012). In order to assess the performance of the IWV estimates from GNSS observations, the uncertainty of the reference values must be quantified. Enhancing the approach followed by Liu et al. (2000) the proposed approach takes into consideration the correlation between the IWV of the neighboring atmospheric layers, thus it gives a more realistic estimate for the uncertainty.

Table 1 shows that at the vast majority of the radiosonde launching sites the Vaisala RS-92 sondes are used. The technical specification of the radiosonde (Vaisala 2010) provides the total uncertainty of temperature, pressure and relative humidity as ± 0.5 °C, ± 1 hPa and ± 2.5 % respectively (2σ). In this study all the derived numerical values are based on the official Vaisala technical specification. However, it must be noted that Miloshevich et al. (2009) showed based on an intercomparison campaign that the accuracy of the relative humidity observations are 3 % and 4 % (1σ) for nighttime and daytime observations respectively. The diurnal difference is caused by the radiation dry bias of the radiosondes (Vömel et al. 2007).

Although the used radiosonde instrumentations have been changed during the study period at least two-three times (RS-80; RS-90; RS-92), our aim is to quantify the uncertainty of the IWV results for the future observations based on the real atmospheric conditions. Therefore throughout the analysis the uncertainty measures of the Vaisala RS-92 are used and the different meteorological conditions are modeled with archive radiosonde profiles.

In order to compute the uncertainty of the IWV calculated from the radiosonde profiles, the law of error propagation is applied to each step of the calculation introduced in Sect. 4.1.

The uncertainty of the saturated water vapour is computed using the derivative of Eq. (11) with respect to the temperature T:

$$\frac{\partial e_w}{\partial T} = 6.112 \left[\frac{17.62}{T + 243.12} - \frac{17.62T}{(T + 243.12)^2} \right] e^{\frac{17.62T}{T + 243.12}}, \tag{16}$$

thus the uncertainty is:

$$\sigma_{e_w} = \sqrt{\left(\frac{\partial e_w}{\partial T} \right)^2 \sigma_T^2}. \tag{17}$$

The partial water vapour pressure can be computed as a function of saturated water vapour and relative humidity [Eq. (12)]. Thus the propagation of uncertainty can be written as:

$$\sigma_{e_v} = \sqrt{RH^2 \sigma_{e_w}^2 + e_w^2 \sigma_{RH}^2}. \tag{18}$$

Since pressure observations are used to compute both the mixing ratio [Eq. (13)] and the IWV [Eq. (14)], the mixing ratios and the pressure observations used in Eq. (14) are

correlated. Thus the integrated water vapour at each layer is written as:

$$IWV_i = \frac{622}{20g}\left(p_{i-1} - p_i\right)\left[\frac{e_{i-1}}{p_{i-1} - e_{i-1}} + \frac{e_i}{p_i - e_i}\right], \tag{19}$$

where p_{i-1}, p_i are the pressure values at the lower and upper boundary of the layer, while e_{i-1} and e_i are the partial pressure of water vapour at the respective boundaries. The aforementioned quantities are supposed to be statistically independent, therefore the uncertainty of the integrated water vapour at layer i can be computed using the following formulae:

$$\sigma_{PWV_i} = \sqrt{\left(\frac{\partial IWV_i}{\partial p_{i-1}}\right)^2 \sigma_{p_{i-1}}^2 + \left(\frac{\partial IWV_i}{\partial p_i}\right)^2 \sigma_p^2 + \left(\frac{\partial IWV_i}{\partial e_{i-1}}\right)^2 \sigma_{e_{i-1}}^2 + \left(\frac{\partial IWV_i}{\partial e_i}\right)^2 \sigma_{e_i}^2} \tag{20}$$

$$\frac{\partial IWV_i}{\partial p_{i-1}} = \frac{622}{20g}\left[\frac{e_{i-1}}{p_{i-1} - e_{i-1}} + \frac{e_i}{p_i - e_i} + \frac{\left(p_{i-1} - p_i\right)e_{i-1}}{\left(p_{i-1} - e_{i-1}\right)^2}\right], \tag{21}$$

$$\frac{\partial IWV_i}{\partial p_i} = -\frac{622}{20g}\left[\frac{e_{i-1}}{p_{i-1} - e_{i-1}} + \frac{e_i}{p_i - e_i} + \frac{\left(p_{i-1} - p_i\right)e_i}{\left(p_i - e_i\right)^2}\right], \tag{22}$$

$$\frac{\partial IWV_i}{\partial e_{i-1}} = \frac{622}{20g}\left(p_{i-1} - p_i\right)\left[\frac{1}{p_{i-1} - e_{i-1}} + \frac{e_{i-1}}{\left(p_{i-1} - e_{i-1}\right)^2}\right], \tag{23}$$

$$\frac{\partial IWV_i}{\partial e_i} = \frac{622}{20g}\left(p_{i-1} - p_i\right)\left[\frac{1}{p_i - e_i} + \frac{e_i}{\left(p_i - e_i\right)^2}\right]. \tag{24}$$

At the final step, the IWV values in the individual layers are summed up. It must be noted that the neighboring IWV values are correlated, since both of them are functions of p and e at the common boundary level. Thus the covariance of the neighboring IWV values must also be computed. The full variance–covariance matrix can be written as:

Table 1 The catalogue of the radiosonde launch sites in Central and Eastern Europe used in this study (WMO 2007)

WMO ID	City/country	LAT	LON	#Obs	Frequency (h)	Sonde
06610	Payerne (CH)	46.82	6.95	8,954	12	SRS-400
10393	Lindenberg (D)	52.22	14.12	24,007	6	RS-92
10548	Meiningen (D)	50.55	10.37	12,809	6–12	RS-92
10739	Stuttgart (D)	48.83	9.20	13,842	12	RS-92
10771	Garmersdorf (D)	49.43	11.90	19,988	6–12	RS-92
10868	Munich (D)	48.25	11.55	12,422	12	RS-92
11010	Linz/Horsching (A)	48.24	14.18	5,086 from 22/01/2011	24	RS-90
11035	Vienna/Hohe Warte (A)	48.25	16.36	11,906	12	RS-92
11240	Graz/Thalerhof (A)	47.00	17.43	5,228	24	RS-90
11520	Prague/Libus (CZ)	50.00	14.45	24,925	6	RS-92
11952	Poprad/Ganovce (SK)	49.03	20.32	11,840	12	RS-92
12120	Leba (PL)	54.77	17.57	8,926	12	RS-92
12374	Legionowo (PL)	52.40	20.97	9,919	12	RS-92
12425	Wroclaw (PL)	51.12	16.88	8,868	12	RS-92
12843	Budapest/Lorinc (H)	47.43	19.18	11,295	12	RS-80 (currently RS-92)
12982	Szeged (H)	46.25	20.10	5,144	24	RS-80 (currently RS-92)
15120	Cluj-Napoca (RO)	46.78	23.57	4,175	24	RS-90
15420	Bucuresti (RO)	44.50	26.13	9,304	12	RS-90
15614	Sofia (BG)	42.82	23.38	2,227	24	RS-92
16044	Udine (I)	46.03	13.18	14,948	6	RS-92
16080	Milano/Linate (I)	45.43	9.28	14,385	12	RS-92
16144	Bologna/San Pietro (I)	44.65	11.38	6,281	12	RS-92

$$\Sigma_{IWV} = \begin{bmatrix} \sigma^2_{IWV_1} & c_{12} & & & & \\ c_{12} & \sigma^2_{IWV_2} & c_{23} & & & \\ & c_{23} & \sigma^2_{IWV_3} & & & \\ & & & \bullet & & \\ & & & & \bullet & \\ & & & & & \bullet \\ & & & & & \sigma^2_{IWV_{n-1}} \quad c_{n-1,n} \\ & & & & & c_{n-1,n} \quad \sigma^2_{IWV_n} \end{bmatrix}, \tag{25}$$

where σ_{IWV_i} is computed using Eq. (20), and the covariance is:

$$c_{i,i+1} = \left(\frac{\partial IWV_i}{\partial p_i}\right)\left(\frac{\partial IWV_{i+1}}{\partial p_i}\right)\sigma^2_{p_i} + \left(\frac{\partial IWV_i}{\partial e_i}\right)\left(\frac{\partial IWV_{i+1}}{\partial e_i}\right)\sigma^2_{e_i}. \tag{26}$$

Since the total value of the IWV is computed as the sum of the IWV_i values, the variance of the total IWV can be computed as the sum of the elements of the variance–covariance matrix in Eq. (25).

However, the NOAA Radiosonde database contains the dewpoint profiles instead of the relative humidity, therefore the computational procedure must be slightly changed with respect to Eqs. (16)–(26). Since the partial water vapour pressure can be calculated from the dewpoint directly using Eq. (15), therefore the uncertainty of the calculated dewpoint must be estimated.

The partial pressure of the water vapour can be computed from the raw observations using Eqs. (11) and (12). Afterwards the dewpoint is calculated from the following equation:

$$T_d = \frac{243.12 \cdot \ln 6.112 - 243.12 \cdot \ln e_v}{\ln e_v - \ln 6.112 - 17.62} \tag{27}$$

The partial water vapour pressure is function of the observed temperature and the relative humidity, and these observations are assumed to be uncorrelated, therefore the uncertainty of the dewpoint can be derived from Eq. (27):

$$\sigma_{T_d} = \frac{\partial T_d}{\partial e_v}\sigma_{e_v} = \left[-\frac{243.12}{e_v\left[\ln e_v - \ln 6.112 - 17.62\right]} - \frac{243.12 \ln 6.112 - 243.12 \ln e_v}{(\ln e_v - \ln 6.112 - 17.62)^2 e_v}\right]\sigma_{e_v}, \tag{28}$$

where σ_{e_v} can be computed with Eq. (18). Thus, the uncertainty of the input data in the NOAA database is given using the uncertainty provided by Vaisala (2010) and Eq. (28) for the dewpoint.

Based on the uncertainty of the dewpoint, the uncertainty of the partial water vapour pressure can be computed following Eq. (15):

$$\sigma_{e_v} = \frac{\partial e_v}{\partial T_d}\sigma_{T_d} = 6.112\left[\frac{17.62}{243.12 + T_d} - \frac{17.62 T_d}{(T_d + 243.12)^2}\right] e^{\frac{17.62 T_d}{T_d + 243.12}}\sigma_{T_d}. \tag{29}$$

Afterwards the procedure described in Eqs. (19)–(26) can be followed to derive the uncertainty of the IWV values.

Central European radiosonde observations have been used to assess the uncertainty of the IWV under different meteorological situations. Although the observations were taken by different radiosondes over the study period, the differences in the accuracy of the sensors have been neglected in the computations. The reason is that our aim was to predict the uncertainty of the radiosonde observations taken by the current radiosonde types under different meteorological situations observed in the past.

The statistical properties of the uncertainties are presented in Table 2. The results show that the mean value of the overall uncertainty of the IWV is ± 0.26 kg/m^2. A strong seasonal variation can be observed in the results, see e.g. the results of Budapest presented in Fig. 2. The mean value is smaller than the results by Liu et al. (2000), the reason for the difference could be due to the different radiosonde type used in this study, since the older Vaisala RS-80 radiosonde was used by Liu et al. (2000), while this study uses the uncertainty measures of the Vaisala RS-92. Another reason could be the differences in climatic conditions, geographical locations and seasonal variations, since radiosonde observations in Hong Kong were used in Liu et al. (2000), while Central and Eastern European observations are used in this study. It must be noted that the uncertainty reaches the level of (± 0.7 to 0.8) kg/m^2 in summertime, when the IWV increases to the level of 35 kg/m^2. Our results agree well with the results obtained by Nash et al. (2011) during the WMO intercomparison campaign, where the uncertainties of different radiosonde models were between ± 0.65 and ± 1.0 kg/m^2, when the IWV was above 50 kg/m^2.

The observed mean uncertainty values show a weak correlation with the latitude. Higher uncertainties are observed at the stations, which are located on the southern part of the study area (Bucuresti, Sofia, Milano, Udine, Bologna).

It must be noted, that neglecting the correlation between the neighboring layers the calculated mean uncertainty decreases by approximately 75 %.

Table 2 Statistical information on the uncertainty calculations for integrated water vapour at the radiosonde launch sites used in this study during 1994 and 2011

WMO ID	City/country	Minimum uncertainty	Maximum uncertainty	Mean uncertainty	Standard deviation
06610	Payerne (CH)	0.04	0.71	0.17	±0.08
10393	Lindenberg (D)	0.04	0.99	0.23	±0.12
10548	Meiningen (D)	0.04	0.96	0.21	±0.10
10739	Stuttgart (D)	0.03	0.99	0.24	±0.11
10771	Garmersdorf (D)	0.04	0.92	0.23	±0.11
10868	Munich (D)	0.03	0.80	0.23	±0.11
11010	Linz/Horsching (A)	0.04	0.87	0.25	±0.12
11035	Vienna/Hohe Warte (A)	0.04	0.98	0.25	±0.12
11240	Graz/Thalerhof (A)	0.05	0.86	0.28	±0.12
11520	Prague/Libus (CZ)	0.04	0.96	0.26	±0.13
11952	Poprad/Ganovce (SK)	0.03	0.87	0.24	±0.12
12120	Leba (PL)	0.05	0.79	0.24	±0.11
12374	Legionowo (PL)	0.04	0.89	0.26	±0.13
12425	Wroclaw (PL)	0.04	0.96	0.26	±0.12
12843	Budapest/Lorinc (H)	0.05	0.93	0.27	±0.13
12982	Szeged (H)	0.05	0.88	0.28	±0.13
15120	Cluj-Napoca (RO)	0.04	0.88	0.26	±0.13
15420	Bucuresti (RO)	0.04	0.98	0.32	±0.16
15614	Sofia (BG)	0.05	0.98	0.32	±0.15
16044	Udine (I)	0.06	0.98	0.33	±0.14
16080	Milano/Linate (I)	0.05	0.99	0.33	±0.14
16144	Bologna/San Pietro (I)	0.06	0.99	0.33	±0.15

The units are kg/m^2

4.3 The Computation of the Hydrostatic and Wet Delays from the Radiosonde Observations

The accurate modeling of the zenith hydrostatic delay has an utmost importance for the computation of zenith wet delays and for the estimation of the integrated water vapour. The zenith tropospheric delays can be computed based on the refractivity profile using Eq. (2). According to Smith and Weintraub (1953) the wet and the dry refractivity can be separated. Since the partial pressure of dry air in Eq. (1) cannot be observed, this equation is reformulated to express the hydrostatic and wet refractivity:

$$N_H = k_1 \frac{p}{T}, \text{ and} \tag{30}$$

$$N_W = (k_2 - k_1)\frac{e_v}{T} + k_3 \frac{e_v}{T^2}. \tag{31}$$

where p, T and e_v are the total air pressure, the ambient temperature and the partial pressure of water vapour, respectively. Since radiosonde profiles contain the pressure, temperature and partial water vapour pressure profiles, both the hydrostatic and wet refractivity can be calculated using these observations.

The zenith hydrostatic delay is calculated as the integral of the hydrostatic refractivity along the radiosonde profile:

$$ZHD = 10^{-6} \int_{h_0}^{h_T} N_H \, dh, \tag{32}$$

where h_0 and h_T is the altitude of the antenna and the upper boundary of the troposphere, respectively.

The zenith wet delays can be computed by vertically integrating the wet refractivity:

$$ZWD = 10^{-6} \int_{h_0}^{h_{TP}} N_W \, dh, \tag{33}$$

where h_{TP} is the altitude of the tropopause.

In order to assess the quality of the various tropospheric models used in this study, the uncertainty of the ZHD and ZWD derived from the radiosonde observations must also be determined. Let us assume that the meteorological parameters observed by the radiosonde are statistically independent and the uncertainty of the pressure, the ambient temperature and the partial pressure of the water vapour is σ_p, σ_T and σ_e, respectively. In the following calculations the same

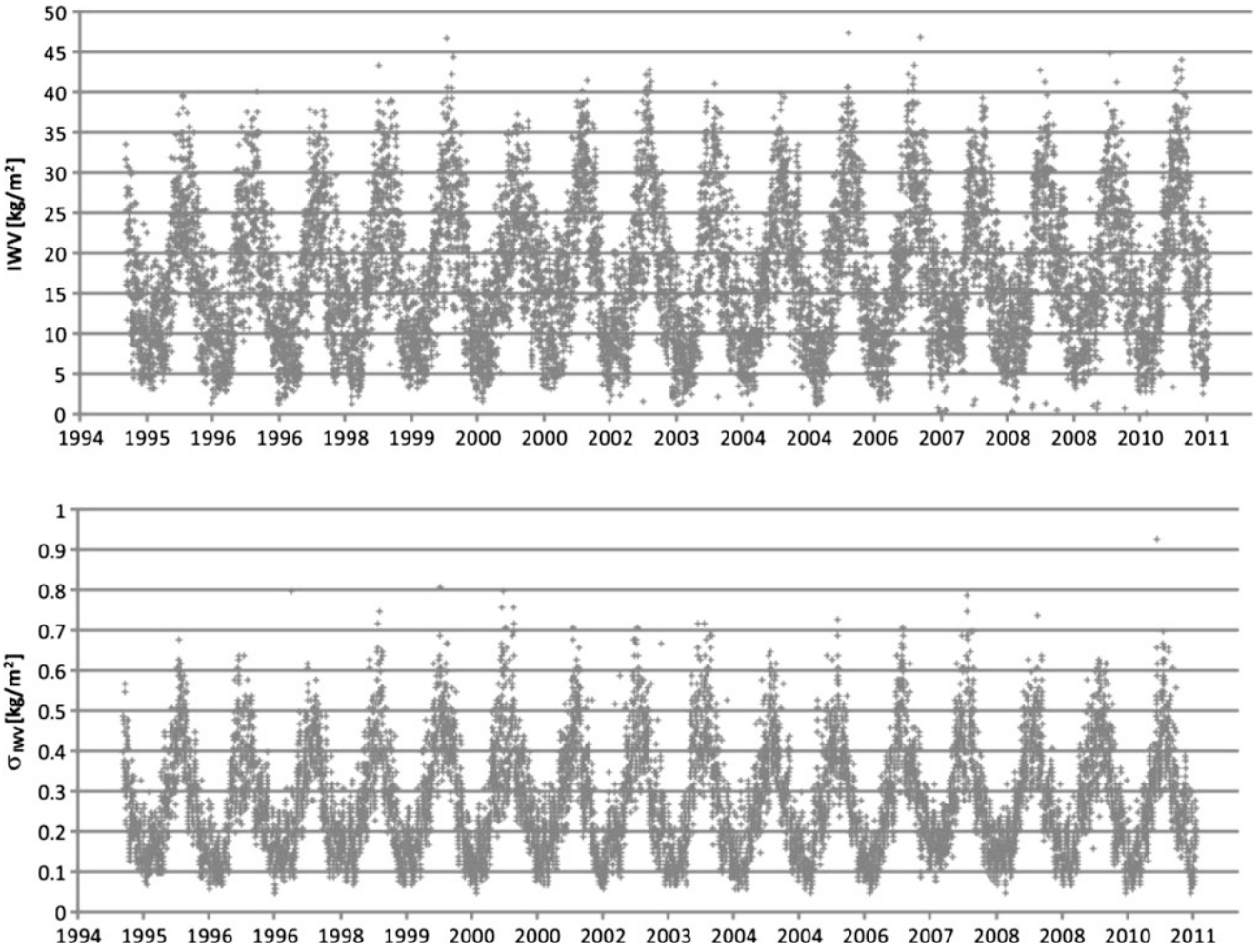

Fig. 2 IWV values (*top*) and their uncertainties (*below*) computed from radiosonde observations at Budapest. The units are kg/m^2

uncertainty values were used for the pressure and temperature as in Sect. 4.2, and the uncertainty of the partial water vapour pressure was computed using the uncertainty of the dewpoint [Eq. (29)].

The uncertainty of the hydrostatic refractivity can be computed using the following equation:

$$\sigma_{N_H} = \sqrt{\left(\frac{k_1}{T}\right)^2 \sigma_p^2 + \left(k_1 \frac{p}{T^2}\right)^2 \sigma_T^2}. \tag{34}$$

The zenith hydrostatic delay caused by an atmospheric layer bounded by the altitudes h_{i-1} and h_i can be calculated by:

$$ZHD_i = 10^{-6} \frac{\left(N_{H_{i-1}} + N_{H_i}\right)}{2} \left(h_i - h_{i-1}\right). \tag{35}$$

Since a similar interlayer correlation can be observed as for the IWV and the total ZHD is computed as the sum of the ZHD_i values, the same approach can be followed as in the previous section.

The full variance–covariance matrix has the same form as Eq. (25), but the variances and the covariances are calculated by the following equations:

$$\sigma_{ZHD_i}^2 = \left[\left(\frac{h_i - h_{i-1}}{2}\right)^2 \left(\sigma_{N_{H_{i-1}}}^2 + \sigma_{N_{H_i}}^2\right) + 2\left(\frac{N_{H_{i-1}} + N_{H_i}}{2}\right)^2 \sigma_h^2\right] 10^{-12}, \tag{36}$$

where σ_h is the uncertainty of the altitude observations. Assuming a radiosonde using GPS code observations for the altitude determination, the uncertainty of ± 5 m was used for the computations.

The covariances between the neighbouring layers are:

$$c_{i,i+1} = \left[\left(\frac{\partial ZHD_i}{\partial N_{Hi}}\right)\left(\frac{\partial ZHD_{i+1}}{\partial N_{Hi}}\right)\sigma_{N_{Hi}}^2 + \left(\frac{\partial ZHD_i}{\partial h_i}\right)\left(\frac{\partial ZHD_{i+1}}{\partial h_i}\right)\sigma_{h_i}^2\right] 10^{-12}. \tag{37}$$

The variance of the zenith hydrostatic delay calculated from a radiosonde profile can be calculated as the sum of the elements of the variance–covariance function. The results of the uncertainty calculations showed that the zenith hydrostatic delay could be computed with the mean uncertainty of ±0.5 mm up to the burst altitude of the balloon. The standard deviation of the uncertainties was ±0.08 mm.

It must be noted that the total zenith hydrostatic delay cannot be computed from radiosonde observations, since the burst altitude of the balloons is usually lower than the altitude of the upper boundary of the troposphere. The burst altitude is between 20 and 35 km depending on the meteorological situation. Thus the delays caused by the upper atmosphere must also be taken into account to obtain consistent results. In this study the International Standard Atmosphere (ISA) (International Organization for Standardization 1975) was used to quantify this correction. When the radiosondes reach the altitude of 27–36 km, the upper air contribution to the hydrostatic delay reaches the value on the order of 1–2 cm (Rózsa et al. 2012).

Since the burst altitudes of the balloons vary significantly among the observations, the estimated ZHD values have different accuracy. Lower burst altitude causes the omission of the observations at higher elevations, thus the standard atmosphere must be used to model the atmospheric effects in the lower altitudes, which eventually decreases the accuracy of the estimated ZHD. In order to quantify this omission error, the zenith hydrostatic delays have been computed using the radiosonde profiles observed at Budapest (more than 11,000 observations during 1994 and 2011), and from the ISA using the same vertical resolution.

After computing the residuals of the ZHD values at the different altitudes, the standard deviation of these residuals were computed for every 1 km thick layer up to the altitude of 36 km. The results are shown in Fig. 3. It can be clearly seen, that the standard deviation is significantly higher below the tropopause, which is explained by the variability of the water vapour in the lower atmosphere. Figure 3 also shows that the standard deviation values can be estimated by a simple exponential function above the 10 km altitude. This would enable the quantification of the omission error as a function of the burst altitude of the radiosonde:

$$\sigma_{ZHDoe} = 0.08921 e^{-1.543 \cdot 10^{-4} H}, \tag{38}$$

where H is the burst altitude in meters, and σ_{ZHDoe} is the omission error expressed in mm.

The results show that the standard deviation of ±1 mm is reached at the level of 29 km, which corresponds to the pressure level of approximately 20 hPa.

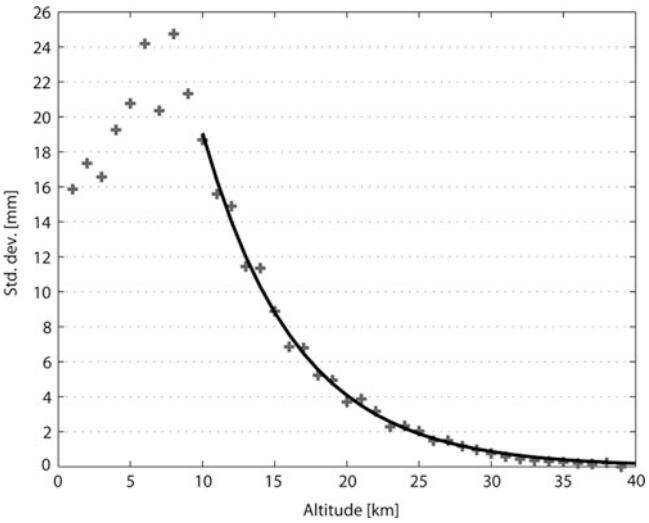

Fig. 3 Standard deviation of the differences between hydrostatic delay values calculated from 10,000 radiosonde launches at Budapest during 1994–2011 and corresponding values calculated from the International Standard Atmosphere, shown as a function of altitude. The units are mm

Zenith wet delays are computed from the radiosonde profiles using Eq. (33). The uncertainty of the radiosonde-based zenith wet delays can be estimated using the same approach as for the ZHD. Firstly, the uncertainty of the wet refractivity must be calculated:

$$\sigma_{N_W} = \sqrt{\left(\frac{k_2 - k_1}{T} + \frac{k_3}{T^2}\right)^2 \sigma_{e_v}^2 + \left(\frac{(k_2 - k_1)\, e_v}{T^2} + 2k_3 \frac{e_v}{T^3}\right)^2 \sigma_T^2}, \tag{39}$$

where the uncertainty of the partial pressure of water vapour can be calculated as a function of the uncertainty of the dewpoint using Eq. (29).

Since the zenith wet delay of the atmospheric layers are calculated as:

$$ZWD_i = 10^{-6} \frac{\left(N_{W_{i-1}} + N_{W_i}\right)}{2} \left(h_i - h_{i-1}\right), \tag{40}$$

the uncertainty of the zenith wet delays can be computed using Eqs. (25), (36), and (37).

Although the zenith wet delay is significantly lower than the zenith hydrostatic delay, the results of the uncertainty calculations showed that the mean uncertainty reaches the level of ±1.5 mm with a similarly strong seasonal variation as experienced in the uncertainty of the IWV. The standard deviation of the uncertainties is ±0.7 mm. This phenomena can be explained with the seasonal variation of the water vapour content of the troposphere.

5 Evaluation of the Functional Models Used for the Estimation of IWV from GNSS Observations

5.1 ZHD Models

The determination of the zenith hydrostatic delay is necessary for the computation of the ZWD delays from the estimated ZTD. Section 4.3 showed that the accuracy of the ZHD derived from radiosonde observations is strongly affected by the burst altitude of the balloon, therefore the zenith hydrostatic delay models were evaluated using radiosonde observations reaching the pressure level of 10 hPa. In total more than 152,000 observations fulfilled this requirement at the 22 radiosonde stations used in this study.

Based on these observations two ZHD models were derived as a linear function of the surface air pressure. The first model (ZHD-M1) is defined by:

$$ZHD = 2.2766 \cdot 10^{-3} p, \tag{41}$$

while the second model (ZHD-M2) contains a bias parameter, too:

$$ZHD = a_0 + a_1 p, \tag{42}$$

where $a_0 = (-0.0027 \pm 0.0003)$ m and $a_1 = (2.2793 \cdot 10^{-3} \pm 3.1 \cdot 10^{-7})$ m/mbar.

The performance of ZHD-M1 and ZHD-M2 were compared to the models by Saastamoinen (1972, 1973), Hopfield (1969) and Black (1978) for the station Budapest and the period 2011, April 14 to June 6. The estimated ZHD values were compared with the ZHD retrieved from the radiosonde observations including the correction for the upper air contribution. Statistical information on the residuals is presented in Table 3. The results show that the Saastamoinen model and the two local models (ZHD-M1 and ZHD-M2) fitted best to the radiosonde observations in terms of standard deviation, while the ZHD-M2 showed the smallest bias of only 0.8 mm, which corresponds to less than 0.2 kg/m^2 bias in the estimated IWV.

Table 3 Statistical information on the comparison of five ZHD-models with respect to ZHD calculated from integration through radiosonde profiles

Model	Minimum difference	Maximum difference	Mean difference	Standard deviation
Saastamoinen (1972, 1973)	−4.5	2.3	−1.5	±1.2
Hopfield (1969)	−5.1	5.6	−0.9	±2.1
Black (1978)	−2.7	8.5	1.8	±2.3
ZHD-M1 (this paper)	−4.1	2.7	−1.1	±1.2
ZHD-M2 (this paper)	−3.8	3.0	0.8	±1.2

The units are mm

5.2 The Models Used for the Determination of the Scale Factor Between IWV and ZWD

After the ZWD is computed from the ZTD and the ZHD, the IWV is calculated using a scale factor defined in Eq. (8). In this paper two approaches are tested. The first approach is proposed by Bevis et al. (1992), where the mean temperature of the water vapour is estimated as a linear function of the surface temperature [Eq. (9)]. Afterwards the Q scale factor is computed using Eq. (8). Another approach is proposed by Emardson and Derks (2000), where a polynomial model of the surface temperature is used for calculating the inverse of the scale factor Q.

More than 17 years of radiosonde observations in Central and Eastern Europe are used for the evaluation of the existing scale factor models as well as for the derivation of two new local models. The ZWD and the IWV values are calculated from the radiosonde profiles according to the methodology introduced in Sect. 4. Afterwards the scale factor Q is calculated as the ratio between the computed IWV and the ZWD. Assuming an IWV of 30 kg/m^2 and the corresponding ZWD of 195 mm, the uncertainty of the radiosonde-based scale factor can be estimated using the uncertainties of the ZWD and IWV given in Sect. 4. The results show that the estimated uncertainty of the scale factor Q is in the order of ±0.001, which corresponds to the relative uncertainty of ±0.6 %.

Two new local models are determined using the radiosonde observations. The Scale-Factor-Model-1 (SFM-1) is derived according to the approach proposed by Bevis et al. (1992). On the other hand the Scale-Factor-Model-2 (SFM-2) is determined following the approach proposed by Emardson and Derks (2000) in their polynomial model.

The Scale-Factor-Model-1

Those radiosonde observations from all of the 22 stations where the observations reached the pressure level of 10 hPa were analysed to derive this model. The mean temperature of the water vapour was computed for each profile and a linear regression function has been established between the surface temperature and the T_m (Fig. 4):

$$T_m = 75.986 + 0.697 T_s. \tag{43}$$

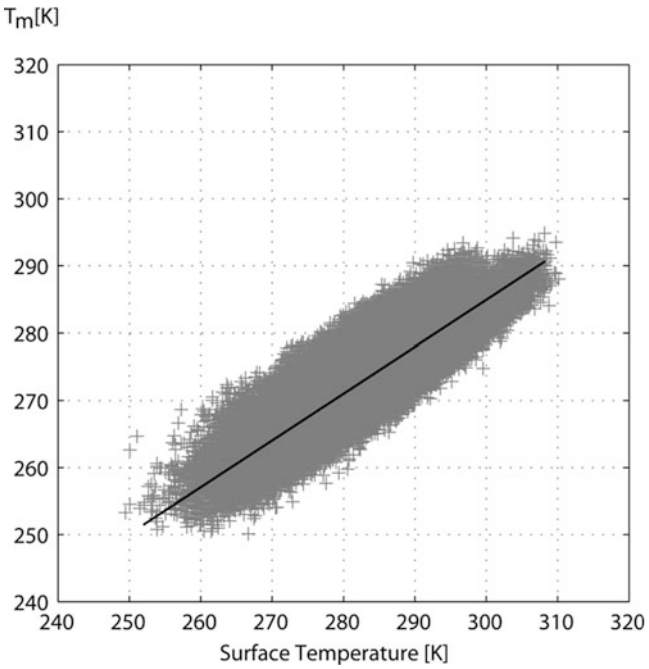

Fig. 4 Scatter plot of the surface temperature (T_s) and the mean temperature of water vapour (T_m). The bold line is the fitted regression line

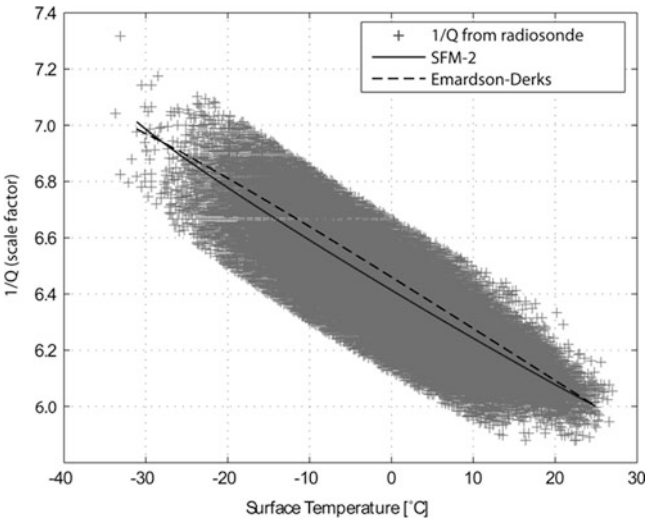

Fig. 5 Scatter plot of the scale factor Q^{-1} and the surface temperature. The dashed curve represents the original polynomial model of Emardson and Derks (2000), while the black line shows the model fitted to Central-European radiosonde observations

It must be noted that the parameters are slightly different than those given by Bevis et al. (1992). The differences can be explained by the different geographical location as well as the amount of the radiosonde profiles used for the derivation of the SFM-1 model.

The Scale-Factor-Model-2

The same atmospheric profiles were used for the derivation of the SFM-2. The ZWD values as well as the IWV values were computed from the radiosonde observations, thus the scale factor Q could be calculated directly from the ratio of the computed IWV and ZWD. In this way a second order polynomial of the surface temperature could be fitted to the computed scale factors following the approach proposed by Emardson and Derks (2000). Figure 5 shows the distribution of the Q^{-1} values (the ZWD/IWV ratio) as a function of the surface temperature. The SFM-2 can be described with the polynomial proposed by Emardson and Derks (2000):

$$Q = \frac{1}{a_0 + a_1\left(T_s - \overline{T}\right) + a_2\left(T_s - \overline{T}\right)^2}, \qquad (44)$$

where the parameters of the polynomial are $a_0 = (6.3953 \pm 0.0003)$, $a_1 = (-1.75 \times 10^{-2} \pm 2.7 \times 10^{-5})\,\mathrm{K}^{-1}$, $a_2 = (7.5 \times 10^{-5} \pm 2.5 \times 10^{-6})\,\mathrm{K}^{-2}$.

Emardson and Derks (2000) proposed the following model parameters: $a_0 = (6.458 \pm 0.0002)$, $a_1 = (-1.78 \times 10^{-2} \pm 2 \times 10^{-5})\,\mathrm{K}^{-1}$, $a_2 = (-2.2 \times 10^{-5} \pm 2 \times 10^{-6})\,\mathrm{K}^{-2}$. It can be seen that the major difference is that the a_2 parameter of the SFM-2 model has the opposite sign compared to the original polynomial model proposed by Emardson and Derks (2000).

Table 4 Comparison of inverse scale factors (Q^{-1})

Model	Minimum difference	Maximum difference	Mean difference	Standard deviation
Bevis et al. (1992)	−0.247	0.369	0.040	±0.092
Emardson and Derks (2000)	−0.344	0.289	0.061	±0.092
SFM-1 (this paper)	−0.311	0.317	−0.020	±0.092
SFM-2 (this paper)	−0.277	0.277	0.000	±0.092

The results derived from four models are compared to reference values based on direct calculation using radiosonde profiles (quantities are unitless)

The Evaluation of the Scale Factor Models

The performance of the four models (Bevis et al. 1992; Emardson and Derks 2000; SFM-1; SFM-2) was evaluated using 152,000 radiosonde observations in Central and Eastern Europe. The inverse scale factors Q^{-1} calculated from the four models were compared to a common reference that was calculated directly from the radiosonde profiles. Statistical information on this comparison is presented in Table 4. The models by Bevis et al. (1992) and Emardson and Derks (2000) show positive biases of 0.040 and 0.061 for the inverse scale factor, respectively. This means e.g. that GNSS-based IWV estimates in Central Europe that are derived using the model by Bevis et al. (1992) and Emardson and Derks (2000) have positive biases of about 0.6 % and 1 %, respectively (biases of 0.2 and 0.3 kg/m^2 or a IWV of 30 kg/m^2, respectively).

SFM-1 shows a negative bias of −0.020, while SFM-2 does not show any bias. This shows that the two-step approach following Bevis et al. (1992) that was used to derive SFM-1 performs worse than the approach by Emardson and Derks (2000) that was used to derive SFM-2.

Table 4 shows that the standard deviations are on the same level for all of the models, this means that the relative uncertainty is approximately ±1.4 %. Since the reference values of the scale factor had the relative uncertainty of ±0.6 %, therefore the relative uncertainty of the models are in the order of ±1.2 %.

The conclusion from this comparison is that SFM-2 should be used in Central and Eastern Europe.

6 Conclusions

As a result of the presented studies, an optimum processing scheme for the estimation IWV retrieved from GNSS observations can be formulated. This processing scheme includes three steps. In the first step, GNSS data need to be processed to derive ZTD. Step two is to calculate corresponding ZHD based on observed surface pressure using a local model which is determined from radiosonde observations in the region of interest. We showed that local ZHD models give biases as low as 0.8 mm for the ZHD. The burst altitude of the radiosondes plays an important role, and we showed that the uncertainty caused by the omitted contributions in the upper atmosphere can be modeled with an exponential model. In step three the ZWD is calculated from subtracting ZHD from ZTD, and the resulting ZWD is converted to IWV. The conversion factor needed for this calculation should be modeled based on surface temperature, while the necessary model parameters should be derived from radiosonde observations in the region of interest. We showed that such a local model for the conversion factor gives zero bias and a standard deviation corresponding to 1.5 % in IWV.

Our results show that using radiosonde observations in the region of interest for both the model to calculate ZHD as a function of surface pressure and the scale factor to scale from ZWD to IWV proves to give the best agreement with IWV directly calculated from radiosonde observations.

Another result of these studies is the uncertainty of IWV derived from radiosonde observations. This uncertainty is derived from error propagation taking into account the interlayer correlation of the IWV. Using more than 276,000 radiosonde observations in Central Europe the average uncertainty is ±0.26 kg/m^2. However, this value shows a strong seasonal variation. The calculated uncertainties agree well with previous studies comparing microwave radiometer and GNSS results (e.g. Niell et al. 2001).

ZTD derived from GNSS has an uncertainty of about ±7 mm (Pacione and Vespe 2008) based on the intercomparison of different GNSS processing schemes, corresponding to ±1.1 to 1.2 kg/m^2 in the IWV (Rózsa et al. 2012). Thus, IWV derived from GNSS has a slightly higher uncertainty than the IWV derived from radiosondes in summertime (±0.7 to 0.8 kg/m^2).

Since the ZHD models show a bias between +0.8 and −1.8 mm, therefore the GNSS derived IWV is biased by between −0.1 and +0.2 kg/m^2 depending on the model used to calculate ZHD. The results showed that the bias caused by the ZHD models can be reduced by 50 % when local ZHD models are used.

Acknowledgements The author acknowledges the support of the Hungarian Scientific Research Fund within the framework of project K-83909.

This work is connected to the "Development of quality-oriented and harmonized R + D + I strategy and functional model at BME" project. This project is supported by the New Hungary Development Plan (Project ID: TÁMOP-4.2.1/B-09/1/KMR-2010-0002).

The valuable comments of the anonymous reviewers are greatly appreciated. They helped to significantly improve the quality of the manuscript.

References

Bevis M, Businger S, Herring TA, Rocken C, Anthes A, Ware R (1992) GPS meteorology: remote sensing of atmospheric water vapour using the global positioning system. J Geophys Res 97:15787–15801

Black HD (1978) An easily implemented algorithm for the tropospheric range correction. J Geophys Res 83:1825–1828

Bosy J, Rohm W, Sierny J (2010) The concept of near real time atmosphere model based on the GNSS and meteorological data from the ASG-EUPOS reference stations. Acta Geodyn Geomater 7:253–263

Boehm J, Werl B, Schuh H (2006) Troposphere mapping functions for GPS and very long baseline interferometry from European Centre for Medium-Range Weather Forecasts operational analysis data. J Geophys Res 111:B02406. doi:10.1029/2005JB003629

Dach R, Hugentobler U, Fridez P, Meindl M (2007) Bernese GPS software version 5.0. Astronomical Institute, University of Bern, Bern

Dow JM, Neilan RE, Rizos C (2009) The international GNSS service in a changing landscape of global navigation satellite systems. J Geod 83:191–198. doi:10.1007/s00190-008-0300-3

Emardson TR, Derks HJP (2000) On the relation between the wet delay and the integrated water vapour in the European atmosphere. Meteorol Appl 7:61–68

Hofmann-Wellenhof B, Lichtenegger H, Wasle E (2008) GNSS: global navigation satellite systems. Springer, Wien New York

Hopfield HS (1969) Two-quartic tropospheric refractivity profile for correcting satellite data. J Geophys Res 74:4487–4499

Igondova M, Cibulka D (2010) Integrated water vapour and Zenith Total Delay time series and models over Slovakia and vicinity. Contrib Geophys Geod 40:299–312

International Organization for Standardization (1975) ISO2533:1975 Standard Atmosphere. ISO

Karabatic A, Weber R, Haiden T (2011) Near real-time estimation of tropospheric water vapour content from ground based GNSS data and its potential contribution to weather now-casting in Austria. Adv Space Res 47:1691–1703

Liu Y, Chen Y, Baki Iz H (2000) Precision of integrated water vapour from radiosonde data for GPS solutions. Geomatica 54:171–175

Miloshevich LM, Vömel H, Whiteman DN, Leblanc T (2009) Accuracy assessment and correction of Vaisala RS92 radiosonde water vapour measurements. J Geophys Res 114:11305–11327. doi:10.1029/2008JD011565

Nash J, Oakley T, Vömel H, Wei L (2011) WMO intercomparison of high quality radiosonde systems. WMO instruments and observing methods, Report no. 107

Niell AE (1996) Global mapping functions for the atmosphere delay at radio wavelengths. J Geophys Res 111:3227–3246

Niell A, Coster A, Solheim F, Mendes V, Toor P, Langley R, Upham C (2001) Comparison of atmosphere wet delay by radiosonde, water vapour radiometer, GPS and VLBI. J Atmos Oceanic Technol 18:830–850

Pacione R, Vespe F (2008) Comparative studies for the assessment of the quality of Near-Real-Time GPS-derived atmospheric parameters. J Atmos Oceanic Technol 25:701–714

Rózsa S (2011) Estimation of integrated water vapour from GNSS observations using local models in Hungary. IAG Symp Ser 136:817–824

Rózsa S, Weidinger T, Gyöngyösi AZ, Kenyeres A (2012) The role of the GNSS infrastructure in the monitoring of atmospheric water vapour. Időjárás Q J Hung Meteorol Serv 116:1–20

Saastamoinen J (1972) Contributions to the theory of atmospheric refraction—part I. Bull Géodésique 105:279–298

Saastamoinen J (1973) Contributions to the theory of atmospheric refraction—part II. Bull Géodésique 107:13–34

Smith EK, Weintraub S (1953) The constants of the equation for atmospheric refractive index at radio frequencies. J Res Natl Bur Stand 50:39–41

Thayer GD (1974) An improved equation for the radio refractive index of air. Radio Sci 9:803–807

Vaisala (2010) Vaisala Radiosonde RS92-D. Technical Data. Ref. B210763EN-B. http://www.vaisala.com/Vaisala%20Documents/Brochures%20and%20Datasheets/RS92-D-Datasheet-B210763EN-B-LoRes.pdf. Accessed 20 Oct 2012

Vömel H, Selkirk H, Miloshevich LM, Valverde-Canossa J, Valdés J, Kyrö E, Kivi R, Stolz W, Peng G, Diaz JA (2007) Radiation dry bias of the Vaisala RS-92 humidity sensor. J Atmos Oceanic Technol 24:953–963

World Meteorological Organization (WMO) (2007) Observing stations and WMO catalogue of radiosondes WMO-No. 9, vol A. http://www.wmo.int/pages/prog/www/ois/volume-a/vola-home.htm. Accessed 20 Oct 2012

World Meteorological Organization (WMO) (2008) Guide to meteorological instrument and methods of observations. WMO-No. 8